

Incorporation of Automated Ball Indentation Methodology for Studying Powder Bed Fabricated 304L Stainless Steel

Sreekar Karnati, Jack Hoerchler, Aaron Flood, Frank Liou

Department of Mechanical and Aerospace Engineering, Missouri University of Science and
Technology, Rolla, MO 65409

Abstract

Automated Ball Indentation (ABI) is a viable method for estimating the ductility, yield stress, and ultimate stress, among other metrics, in different metallic materials. Currently, ABI data analysis utilizes Holloman's Power Law to model the plastic region of the true stress-true strain curve. While this formulation is accurate for some materials, its relevance for additively manufactured austenitic stainless steels, such as 304L, needed investigation. The deviation of the material's plastic behavior from the Power Law was investigated. In order to better model this behavior, both the Voce and Ludwigsen formulation were investigated. These formulations were tested for both wrought and additively manufactured 304L stainless steel. Regression analysis was used to choose the appropriate fit. The chosen formulation was then used to generate a material model to simulate the ABI process. These simulations were validated through experimental analysis.

Introduction

Traditionally, metal components for various engineering applications are fabricated from a raw stock material, through steps of machining and assembly. The choice of raw material usually depends on the requirements of the engineering application. The properties of these raw materials are established through extensive characterization. Post-fabrication, the same stock properties are expected from the machined and assembled components. This approach has been successful and is widely used to date. However, the buy to fly ratios for fabricating components in this manner can be high. Especially, fabricating components from tough and expensive materials can be challenging. As a solution, Additive manufacturing has been identified as a potential means to fabricate such components in an economical fashion.

Additive Manufacturing (AM) is capable of fabricating traditionally infeasible complex geometries from multiple varieties of material. It is also fundamentally different from the traditional approaches. Instead of removing material from a raw stock, AM lets one fabricate individual components piece by piece by adding material in a layer by layer fashion. Unlike conventionally used subtractive manufacturing, the properties of the AM parts cannot be traced back to stock material. Additionally, AM materials/parts have been known to possess excellent yet anisotropic properties. The properties of AM material have been known to vary with attributes such as part size, build strategy, laser power, scan speed etc. [1–6]. The lack of the possibility to trace back the properties to a stock material and the wide variation within the material makes part inspection and qualification quite challenging.

Destructive testing of AM components to assess the influence and variation caused by the various attributes of the fabrication process can be cost prohibitive, counterproductive and difficult. In order to economically investigate the material performance of AM material, miniature tensile testing was utilized [7–9]. While miniature tensile testing was successful in characterizing AM material, it is still a destructive mode of testing. The relevance of these results may also be questioned as it is suspected that the part geometry has an influence on part properties. If the geometry from which the mini-tensile specimens were sampled, happens to be substantially different from the part under scrutiny, the data from mini-tensile testing might be invalid. For reasons of such ambiguity, there is a need for non-destructive means to characterize and inspect AM material and components.

Currently, there exists a wide range of capabilities for performing a non-destructive evaluation for inspection and characterization. Techniques involving, acoustic sensors, infrared sensors, X-rays, microwaves, eddy currents, natural frequency etc. are used from routine inspection to characterization[1,10–15]. Automated Ball Indentation (ABI) is one of such non-destructive testing methodologies. It is capable of estimating multiple material properties. ABI techniques utilize ball indentation data and empirical analysis to estimate various mechanical properties. The ABI technique was developed by Haggag *et.al.* and is currently standardized through ASTM[16]. The technique has also been proven to be effective for fracture toughness estimation[17].

Multiple researchers have demonstrated the viability of utilizing the ABI technique to estimate the mechanical properties of metals. It was claimed to be capable of monitoring the structural integrity of components in nuclear, aerospace, chemical and process plants. This was demonstrated by investigating the viability on materials favorite to these industries[18]. The technique was also found to be capable of identifying spatial gradients in material properties from welding[19]. His technique was also capable of identifying the influence of aging time on mechanical properties of Inconel 625 alloy[20]. While the technique shows great promise, the relevance and validity of this technique for every material requires investigation.

In this paper, the validity of the ABI technique for investigating the mechanical properties of powder bed fabricated 304L stainless steel were investigated. The validity of some assumptions central to the empirical analyses involved in processing ABI data was also investigated. For a better understanding of the technique, the indentation process was also simulated using finite element analysis techniques. Mechanical properties gathered from destructive testing were compared with values estimated through ABI testing.

Theory

The ABI technique uses load vs. depth of indentation data gathered from guided loading and unloading cycles of a ball indenter to estimate various material properties. A schematic layout of the empirical analysis involved in estimating yield strength, engineering ultimate strength, strength coefficient, strain hardening exponent and Meyer's index is shown in Figure 1. The equations involved in the empirical analysis are shown in Figure 2.

The depth of indentation data is used to estimate the chordal diameter of indentation. Using the chordal diameter the mean pressure over the indent during the process of indentation is calculated. The mean pressure vs. chordal diameter data is fit to Meyer's law to estimate 'A' parameter and Meyer's index. The 'A' parameter and tensile yield strength of the material are theorized to have a linear empirical relationship. Therefore the 'A' parameter estimated from indentation can be used to estimate the yield strength of the material. The load and chordal diameter data is also used to estimate the true stress and corresponding true plastic strain data, at the end of each loading cycle. These eight points of true stress and strain can be used to model the flow curve and thereby obtain estimates from strength coefficient and strain hardening exponent.

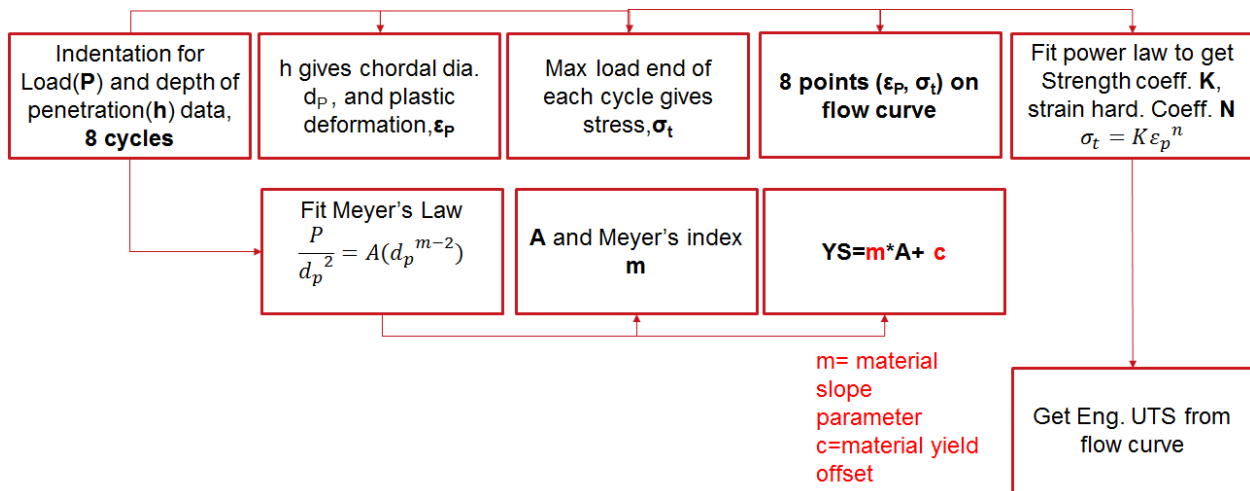


Figure 1. Schematic layout of data processing involved in estimating yield strength, strength coefficient, strain hardening exponent and Meyer's index [16]

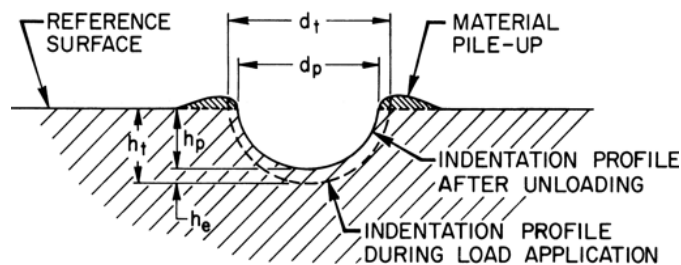


Figure 2. Representation of True (pileup, d_t) and Chordal diameters (in-plane, d_p) of an ABI impression [17].

The Holloman's power law (Equation 1) used to model the plastic portion of the true stress-true strain curve is not an accurate formulation for austenitic stainless steels such as 304L stainless steel. A significant deviation from estimated stress value is noticed for low values of strain. The Ludwigs (Equation 1) and Voce formulations (Equation 3) are more accurate in estimating the full plastic behavior of 304L stainless. This was demonstrated at multiple

temperatures for 316L austenitic stainless steel by Choudary *et.al.*[21]. The equations of the formulations are shown below. Where σ is the calculated true stress, ε_p is the calculated true plastic strain, k, n, k1, n1, A and B are empirical parameters. The parameter ‘n’ from both Ludwigson and Voce formulations is analogous to the strain hardening exponent obtained from the Holloman formulation.

$$\sigma = k(\varepsilon_p)^n \quad \text{Equation 2}$$

$$\sigma = k(\varepsilon_p)^n - e^{(k1-n1(\varepsilon_p))} \quad \text{Equation 3}$$

$$\sigma = B - (B - A)e^{-n\varepsilon_p} \quad \text{Equation 4}$$

<p><i>True plastic strain:</i></p> $\varepsilon_p = \frac{0.2d_p}{D}$	<p><i>Strain range: 0-0.2</i></p> <p><i>Empirical equation by Tador</i></p>
<p><i>True Stress:</i></p> $\sigma_t = \frac{4P}{\pi d_p^2 \delta}$ <p><i>Constraint factor:</i></p> $\delta = \begin{cases} 1.12 & \Phi \leq 1 \\ 1.12 + \tau \ln \Phi & 1 \leq \Phi \leq 27 \\ \delta_{max} & \Phi \geq 27 \end{cases}$	<p>$\Phi = \text{Indentation variable}; \quad \Phi = \frac{\varepsilon_p E_2}{0.43 \sigma_t}$</p> $\delta_{max} = 2.87 \alpha_m$ $\tau = \frac{\delta_{max} - 1.12}{\ln(27)}$ <p>$\alpha_m = \text{Constraint factor index}$</p>
<p><i>Meyer's Law:</i></p> $\frac{P}{d_t^2} = A \left(\frac{d_t}{D} \right)^{m-2}$	<p><i>P= Load</i></p> <p><i>d_t = Total diameter of the indentation</i></p> <p><i>m= Meyer's index</i></p> <p><i>D= Indenter diameter</i></p> <p><i>A= Yield parameter</i></p>
<p><i>Indentation plastic diameter:</i></p> $d_p = \left\{ 0.5CD \left[\frac{h_p^2 + \left(\frac{d_p}{2}\right)^2}{h_p^2 + \left(\frac{d_p}{2}\right)^2 - h_p D} \right] \right\}^{\frac{1}{3}}$	$C = 5.47P \left(\frac{1}{E_1} + \frac{1}{E_2} \right)$ <p><i>E1, E2, are the Young's moduli of the indenter and the test material respectively</i></p> <p><i>h_p, d_p are the plastic depth of indentation and plastic chordal diameter</i></p>
<p><i>Yield stress:</i></p> $\sigma_y = \beta_m A + b_m$	<p><i>Empirical equation by Haggag</i></p> <p><i>β_m is the material yield slope</i></p> <p><i>b_m is the material yield constant</i></p>

Figure 3. Equations involved in the ABI empirical analysis analyses, these equations are used in the sequence shown in Figure 1 [17].

Experimental setup

The stainless steel analyzed in this paper was procured in three states, (1) powder bed fabricated in as-built state, (2) powder bed fabricated and heat treated, and (3) wrought, cold rolled and annealed. The stainless steel fabricated using the laser powder bed fusion process was

produced on a Renishaw AM250 powder bed machine. The parameters used for fabrication were optimized for density and smooth downward facing surfaces. 304L stainless steel powder in the size range of 15-45 micron was used for fabrication. The heat treated material was produced by subjecting the as-built material to 300C for 1 hour. The wrought material was commercially procured.

The ABI indentation was performed using a commercially procured machine. The machine was designed and produced by ABI Services LLC. The indentations were performed using a 0.75mm diameter WC ball indenter. A schematic representation of the loading and unloading cycles is shown in Figure 4. The current implementation of ABI testing involves eight cycles of loading and unloading. Each cycle has the same amount of depth of indentation. The depth of indentation for each cycle is the ratio of peak depth (input as a percentage of the radius of the indenter) and indentation and the total number of cycles (8 cycles). The unloading at the end of each cycle is intended to relieve any elastic deformation and accurately estimate plastic deformation. The Figure 3 highlights the relationship of varying %radius and unloading percentage with load and depth of penetration data.

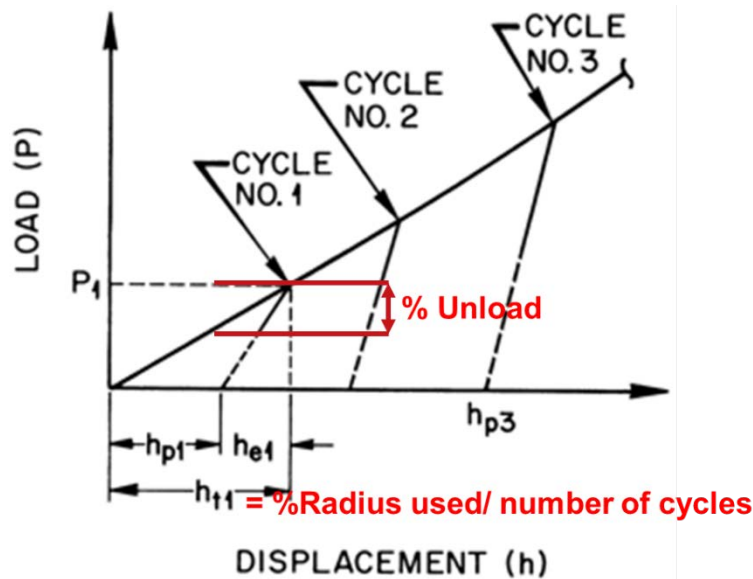


Figure 4. An illustration of the load vs. depth of indentation (displacement) obtained using controlled loading and unloading of a ball indenter[17]

A finite element model was created using ANSYS APDL 18.1 simulation software in order to simulate the plastic deformation occurred during the ball indentation process. Using ANSYS, a script has been written to simulate the ABI testing process. This included a ball indenter situated over a block to be indented on. The ball indenter has been meshed in order to define the contact surface, and the test block has been meshed to optimize accuracy and calculation time using mapped meshing techniques. The meshing schemes are shown together in Figure 5. Contact and Target surfaces have been defined as the areas on the indenter and the top face of the base block respectively. These surfaces will allow for the indenter to deform the target surface on the base block. The ball was meshed using fine free meshing. This allows the program to create a non-uniform map of nodes across the indenter to evenly place nodes on the contact face. The base was meshed with a mapped cubic 8 node mesh. This allowed for a finer mesh to be created closest to

the point of indentation on the block. Doing this improves the quality of the results in the area around the indentation, as well as speeds up calculation time due to fewer elements being used in non-critical locations. A quadratic 20 node 3D element was used to simulate the material behavior during indentation.

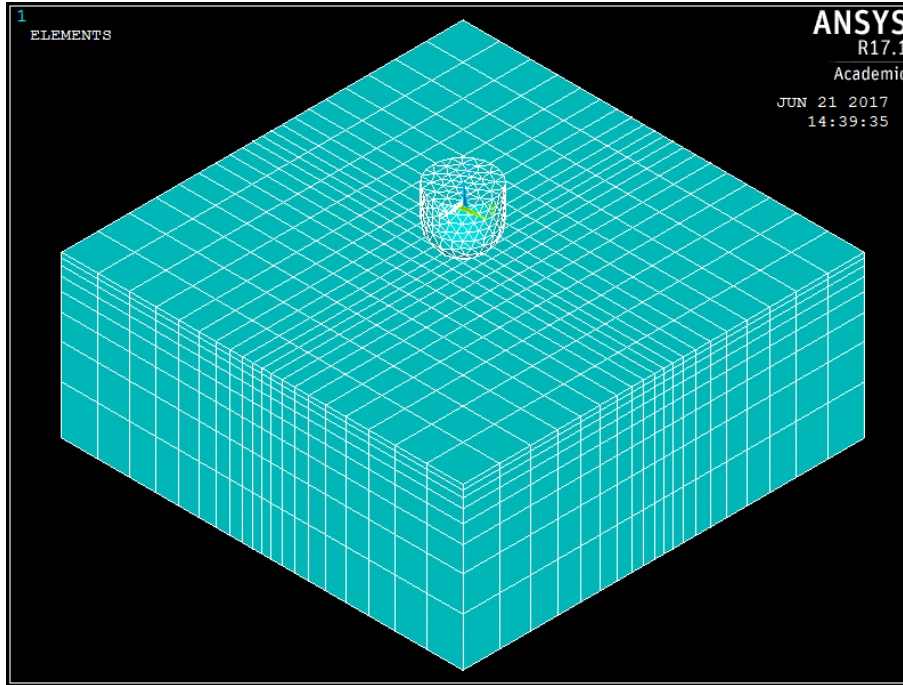


Figure 5. A meshed model of the ball indenter and the test block.

The material parameters of the ball were the same as the values used by the ABI analysis software. The model currently accounts for the material properties of the test block by including modulus of elasticity of 304L (from literature), the nonlinear plastic deformation section of the stress-strain curve (experimental, gathered from testing 6mm X 1mm X 1mm Miniature tensile specimens specimen of SLM material [9]), and the Poisson's ratio of 304L (from literature). The model is set to a constant temperature and temperature dependent properties are ignored due to it having a negligible effect on results. A transient analysis was used to replicate the indentation process. 200-time steps were used in order to displace the indenter in steps down into the block and back up to a position that is clear of the block. These steps were based on the experimental data. The location of the ball during the loading and unloading cycles was identified and used as the input for indentation simulation.

The test block was created to be larger than the interaction volume for ball indentation tests in which the material is affected. This interaction volume was based on the cut-off that plastic deformation wouldn't go beyond twice the diameter of the indenter. This allowed for directly fixed constraints to be used on the outer faces of the block as well as the bottom face of the block. The indenter is fixed above the block base at all of the individual nodes of the block. The indenter is then moved downward/upward in a cyclic fashion over the course of 200 individual steps, end of indentation the indenter moved upward to remove the load on the block. Each step resets the

displacement of the indenter to a new location, moving the indenter. The indenter movement can be realized from the plot shown in Figure 6. This corresponds to an indentation rate of 0.005mm/s.

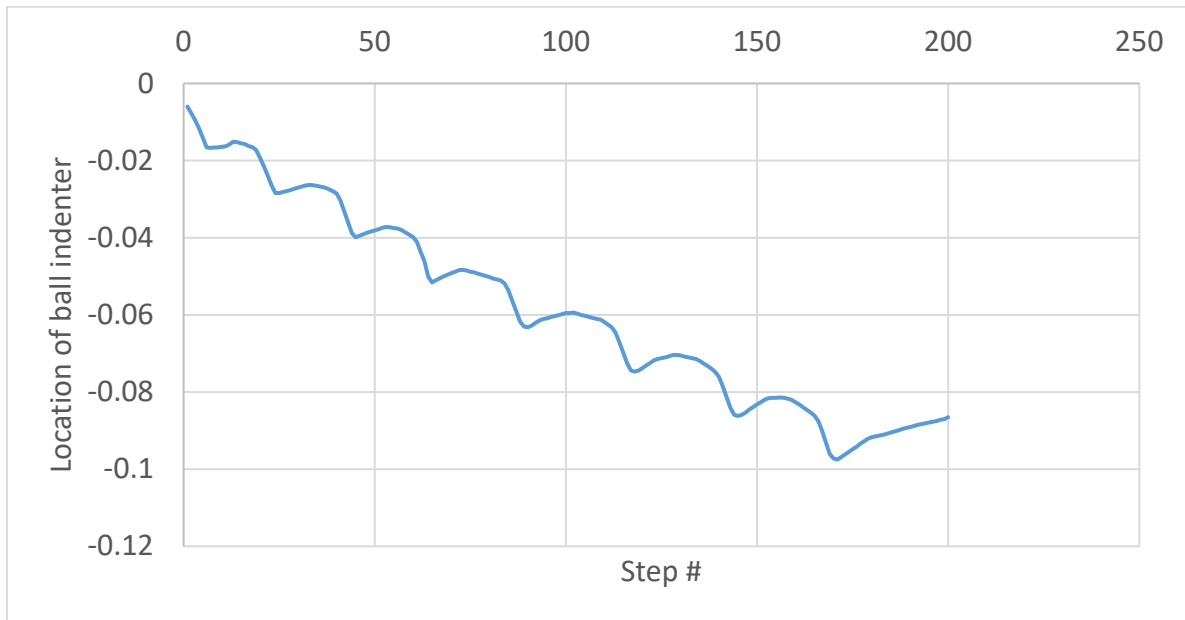


Figure 6. Location of the ball indenter during the course of a 200 step indentation simulation. The peak depth of indentation is 24% of the radius and the total number of loading-unloading cycles are 8.

Results and discussions

Yield strength estimation

The current section of analysis involved the evaluation of the empirical parameters needed to model the linear relationship between ‘A’ parameter and tensile yield strength. The validity of the evaluated model with changing indenter size and changing interaction volume was also investigated. The setup of the linear model between ‘A’ parameter and yield strength data was based on tensile data gathered from as-built AM material and heat treated AM material. Data from 25 specimens in as-built condition [22] and 13 specimens in heat treated condition [23] was used for the setup of the linear model. A set of 3 indentations were performed on each these broken specimens. The ‘A’ parameter gathered from ABI testing and corresponding tensile yield strength measurements were linearly fit to evaluate the empirical constants of the linear relationship. The validity of the obtained fit was cross-checked by comparing indentation and tensile data from a new set of 12 specimens in as-built condition.

ABI literature states the material slope parameter for stainless steels is 0.189 [16], while the intercept value is 0. By forcing the intercept value to be zero, the material slope parameter was found to be 0.1936. However, this was not a good fit. A linear fit with non-zero intercept yielded a good fit. This model was successful in estimating the yield strength values of the second set of indentations. The raw data, the linear fits with zero and non-zero intercepts and their corresponding R^2 values are shown in Figure 7. Although the tensile data spans over a wide range, two clusters

of data points can be seen in the plot. These clusters are representative of the state of the material that was considered in this study. The lower end is the heat treated material and the higher end is the as-built material. The validity of the model for material with properties outside the clusters is yet to be investigated.

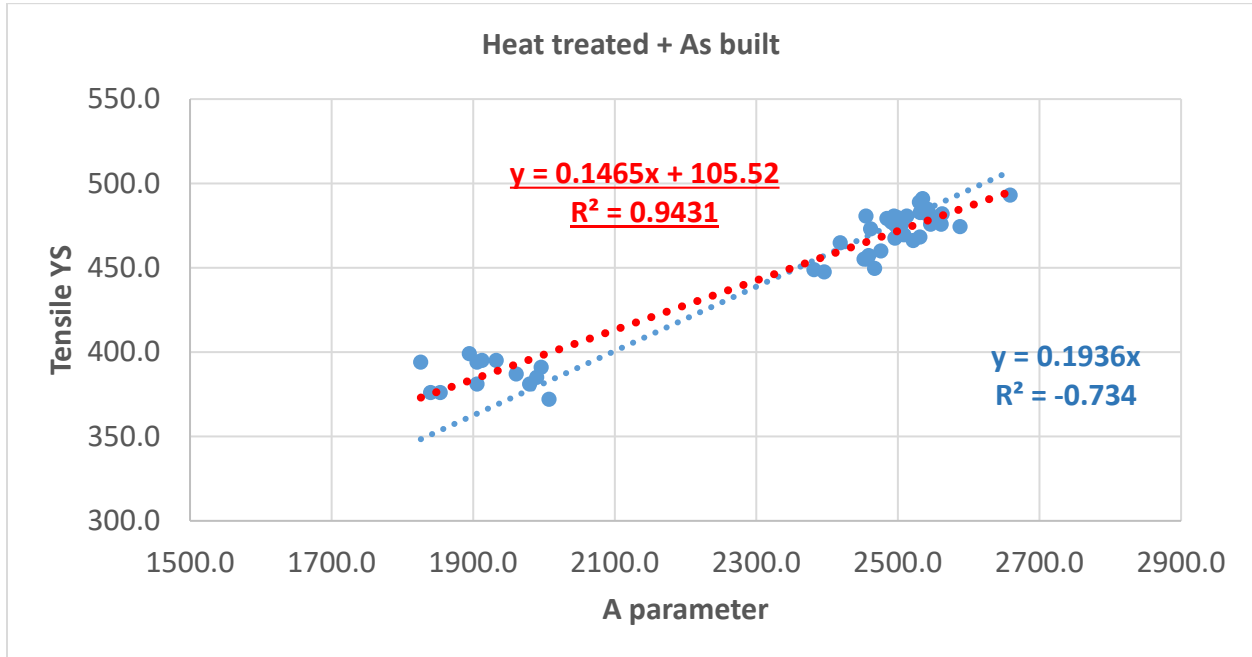


Figure 7. Linear fits between tensile yield strength and A parameter. The fit with non-zero intercept offers good correlation (red)

Table 1. Yield strength measurements taken using tensile testing and their corresponding ABI estimates. Mean and standard deviation in parentheses

Yield Strength (MPa)	
Tensile measured	ABI estimated
500.4	424;458;422;448 (438,15.4)
519.5	433;410;427;405 (418,11.5)
503.8	434;453;424;441 (438, 10.5)

The linear model with the intercept was used as the model estimating yield strength. The new data set gathered to investigate the validity of the model is shown in Table 1. A significant difference can be seen between tensile measurements and ABI estimates. The ABI technique underpredicts the yield strength values. A significant scatter can also be noticed in the ABI estimates. The impact of varying indenter radius on ABI measurements and validity of the linear model at each size was investigated. By increasing the size of the indenter, decreasing values of ‘A’ parameter were obtained. Consequently, lower values of yield strength estimates were

obtained from ABI. The values of ‘A’ parameter and yield strength estimates from ABI linear models are shown in Figure 8. The models with zero and non-zero intercepts were used. A slope of 0.189 was used for the model with zero intercept. The model with non-zero intercept is shown in Figure 7.

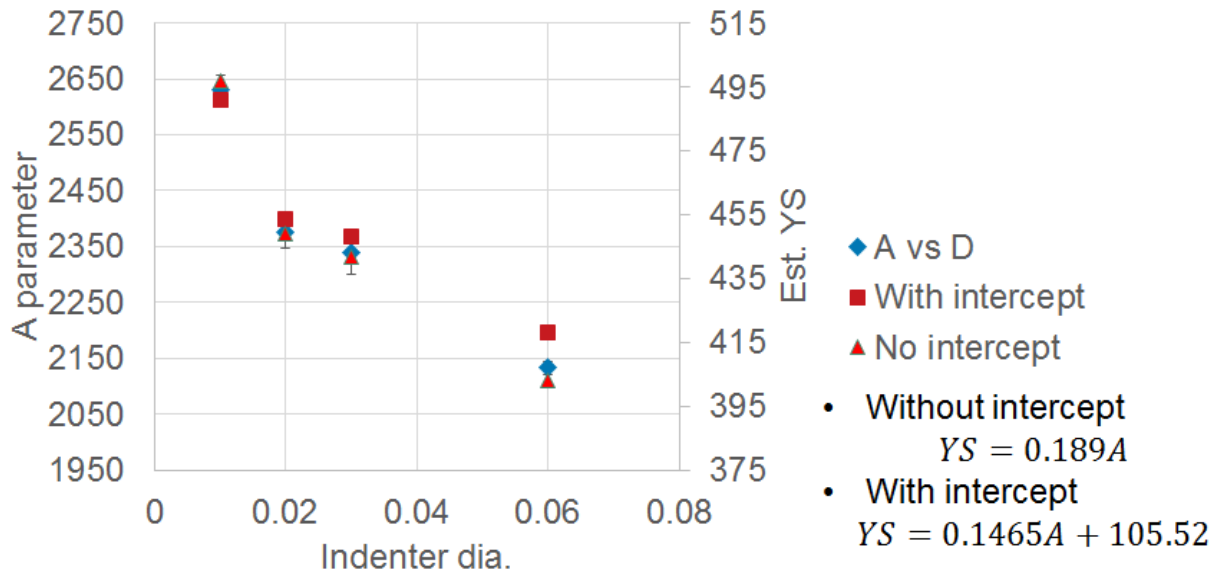


Figure 8. Decreasing values of ABI estimates with increasing indenter diameter

Flow curve formulation

The flow curve modeling is an integral part of the empirical analysis performed by the ABI software. As a default, the Holloman power law is used to model the plastic section of the true stress-true strain curve. However, the power law is not a good representation of the plastic flow of 304L stainless. The same can be seen from the Figure 9. The true stress-true strain data calculated from mini-tensile specimens of 3mm gage length and 1mmx1mm cross-section (both wrought and AM, [9]) were used to fit Ludwigs and Voce models to the plastic portion of the stress-strain curve. While Ludwigs (Equation 4, As-built AM) was better than Holloman fit, it was still not completely representative. Voce model (Equation 5, As-built AM) was found to be the best fit. The same results were seen for both wrought and AM materials. The goodness of it can be seen from the residual plots shown in Figure 10 and Figure 11.

$$\sigma = 1411.1(\epsilon_p)^{0.341} + e^{(5.7-18.2\epsilon_p)} \quad \text{Equation 4}$$

$$\sigma = 2137.2 - (2137.2 - 586.9)e^{-0.964\epsilon_p} \quad \text{Equation 5}$$

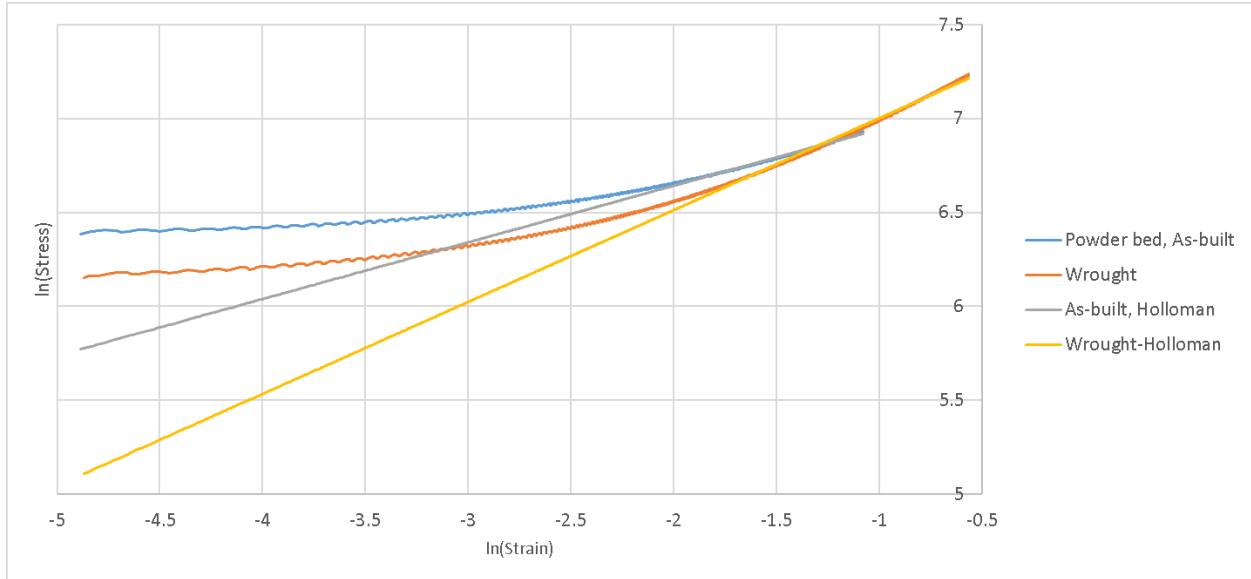


Figure 9. Ln-ln plot of true stress-true strain curves and their Holloman power law fits

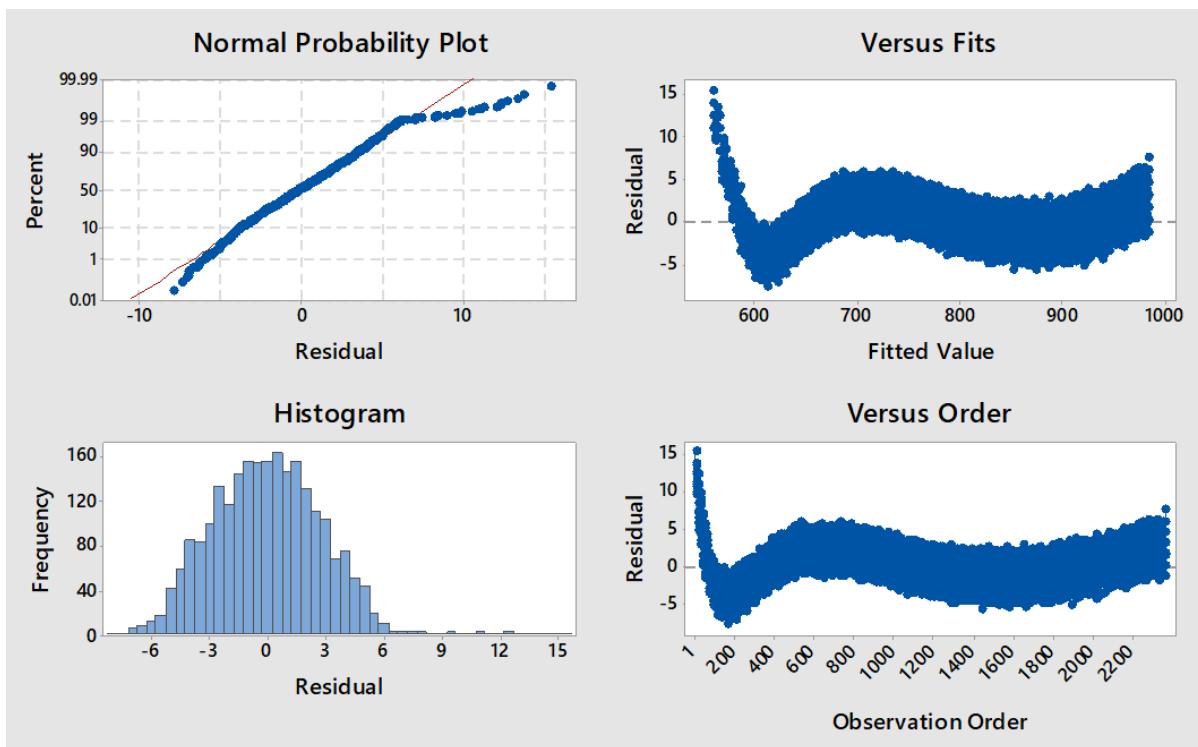


Figure 10. Residual plots of Ludwison model for as-built AM material. The pattern in versus fits and versus order graphs indicate un-modeled data in the residuals.

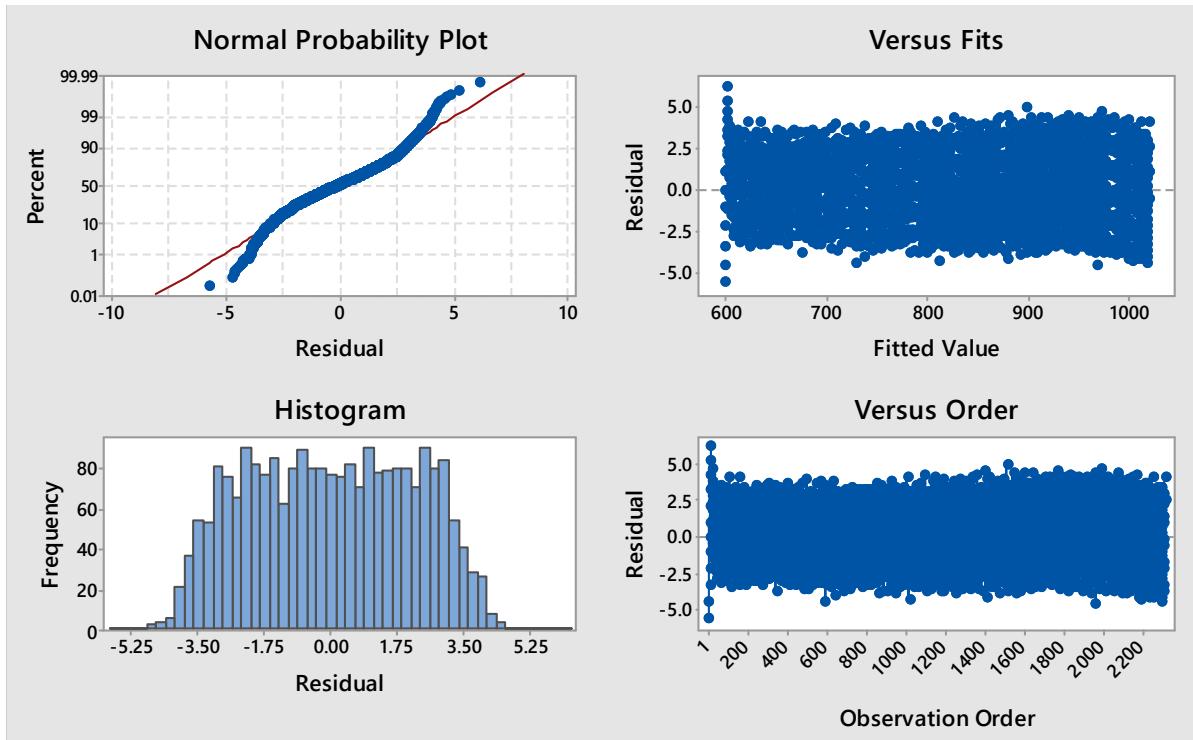


Figure 11. Residual plots of Voce model for as-built AM material. Indicative of a good fit of true stress by using Voce model

Although the Voce formulation is a more accurate fit for modeling the flow curve, it is to be noted that the deviation of the power law from experimental data is only for low values of strain (Figure 9). This means the yield strength estimation from the powder law is infeasible (stress at true plastic strain=0). However, the ultimate strength estimation might still be valid. The power law might be used for strain values higher than a threshold (0.135 mm/mm in this case). The ultimate strength values estimated using the power law are shown in Table 2. While there is still a difference between the measured and estimated values, the difference is low in comparison to yield strength estimation.

Table 2. Ultimate strength measurements taken using tensile testing, and their corresponding ABI estimates

Ultimate Tensile Strength (MPa)	
Tensile measured	ABI estimated (Mean, std. dev.)
673.9	709;708;694;695 (701, 7)
684.6	609;609;661;661 (635, 26)
674.1	655;656;695;695 (675, 19.7)

Finite element method simulation

Currently, all of the material properties used in the simulation are time independent. The modulus of elasticity has been input as 200 GPa, and the Poisson’s ratio has been input as 0.33, both standard values for 304L stainless steel. The exact values of modulus and Poisson ratio of SLM fabricated 304L stainless steel is expected to be different from those of wrought material. For better accuracy, these values are to be experimentally evaluated and inputted into the simulation. Plastic deformation was accounted for by inputting a table to calculate the nonlinear plastic deformation region of the true-stress vs. true-strain curve for 304L, shown in Table 3.

The required number of elements was identified by running simulations with various mesh sizes. The load-displacement (depth of indentation) curve obtained at the end of simulation was used as the norm for identifying the required mesh size. Meshes with total nodes of 20k to 80k were used for simulations. A snapshot of Von Mises stress and Von Mises strain in the test block (80k nodes) and indenter post indentation can be seen in Figure 12. The calculated load-displacement curves from the each of those simulations are shown in Figure 13. The difference between the load values at same positions of the indenter was used to identify convergence. The average and standard deviation of these differences are shown in Table 4. A mesh size of 60K nodes was expected to be sufficient to achieve convergence in estimating the load-depth of indentation plot.

Table 3. True-stress and corresponding true strain values used to model plastic deformation.

True plastic strain (mm/mm)	True plastic stress (MPa)	True plastic strain (mm/mm)	True plastic stress (MPa)
0.00	512.70	0.20	826.18
0.01	550.57	0.22	841.83
0.03	574.16	0.23	855.31
0.04	597.51	0.24	872.67
0.06	615.98	0.26	883.75
0.07	639.15	0.27	901.55
0.08	661.69	0.28	916.04
0.10	680.98	0.31	938.24
0.11	699.52	0.32	955.00
0.12	715.84	0.33	969.54
0.14	738.81	0.34	977.72
0.15	753.31	0.36	991.68
0.16	775.03	0.37	1003.40
0.18	792.43	0.38	1016.37
0.19	808.76		
0.29	929.85		

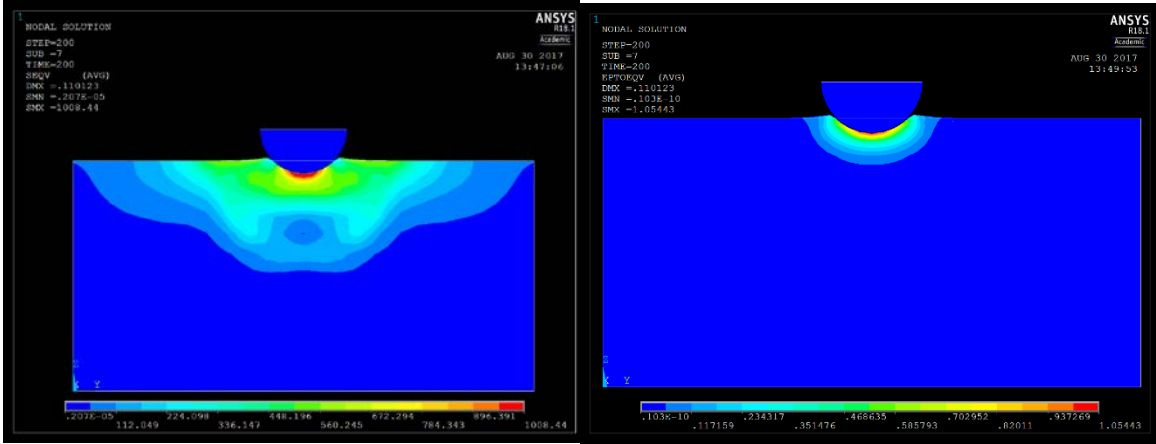


Figure 12. Contour plot of Von Mises stress and strain in the indenter and test block post indentation (mesh size of 80k nodes).

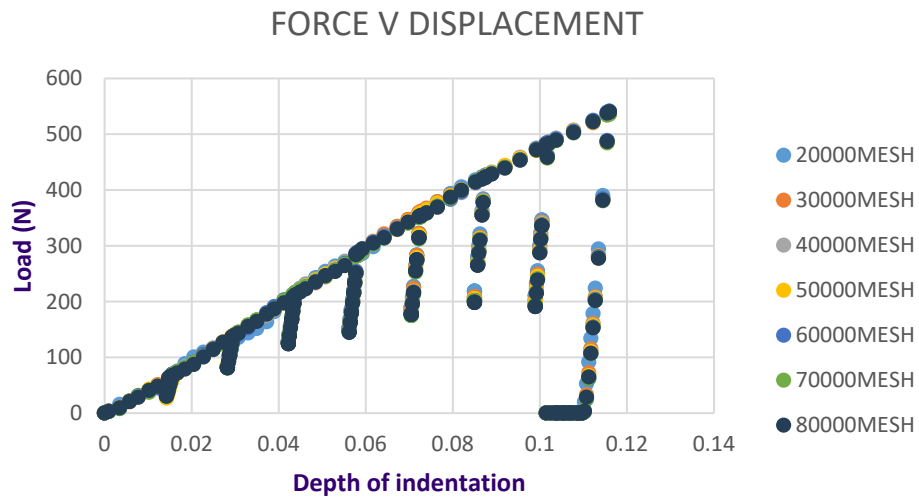


Figure 13. Simulated load-depth of indentation curves obtained through mimicking ABI test on blocks of various mesh sizes.

Table 4. Average and standard deviation of the difference in load values at same depths of indentation for cases shown in Figure 2.10. A mesh size of 60K nodes is expected to achieve convergence

	80k-20k	80k-30k	80k-40k	80k-50k	80k-60k	80k-70k
Mean	5.93	2.94	2.44	2.39	<u>1.63</u>	<u>1.56</u>
Std. Dev	5.89	3.00	2.18	2.07	<u>1.22</u>	<u>1.37</u>

The chordal diameter of the indentation is calculated through an analytical model (see Figure 2 and Figure 3). The estimated value is used for calculating flow stress and plastic strain values. The validity of this estimation is difficult to evaluate as an accurate measurement of chordal/ indentation diameter can prove to be difficult. In order to assess the validity through simulation, convergence needs to be ensured for plastic flow as well. The values of these diameters were calculated from the simulated outcomes discussed above. ImageJ was used to measure the plastic deformation obtained at the end of the simulations. The measured values of these diameters at the end of 1st, 5th and 8th cycle of indentation are shown in Figure 14 and Figure 15.

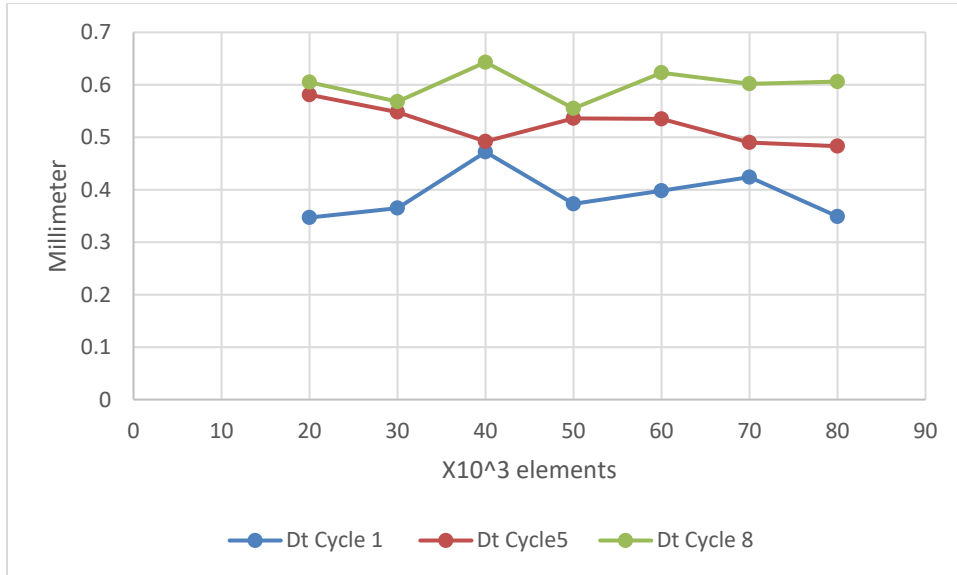


Figure 14. Variation in the measured value of d_t with increasing mesh size.

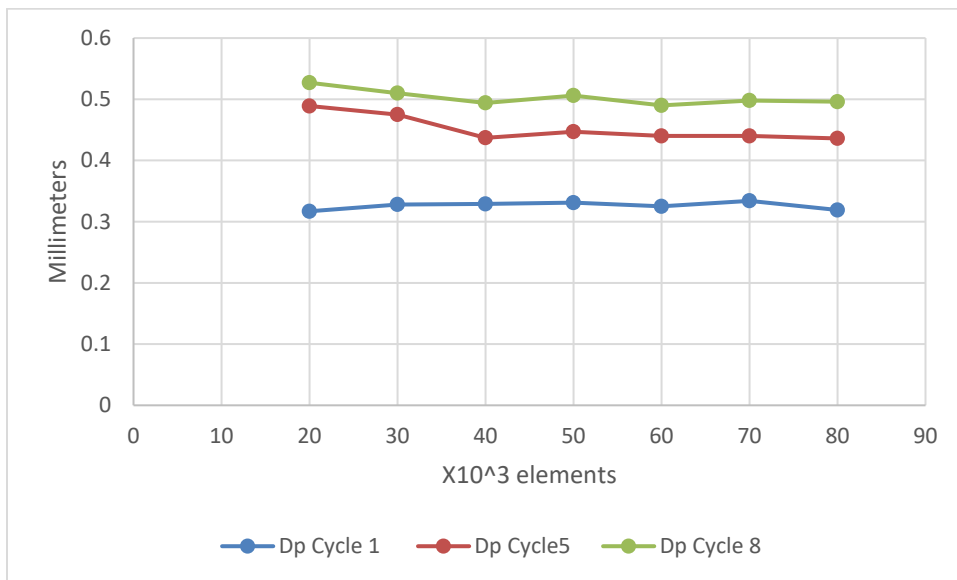


Figure 15. Variation in the measured value of d_p with increasing mesh size.

An overlay of experimental and simulated load vs. depth of indentation curve is shown in Figure 16. A maximum indentation depth of 24% of the indenter radius and an unloading extent of 20% of the peak load at the end of each cycle were used during the simulation and experiment. The spine of the simulated load vs. depth of indentation curve matched very well the experimental data. However, the unloading sections of the curves were not a good match. This mismatch will yield different estimates of chordal diameter and in extension stress, strain, yield, and ultimate strengths. The reason for the mismatch is suspected to be the lack of back stresses in the simulation.

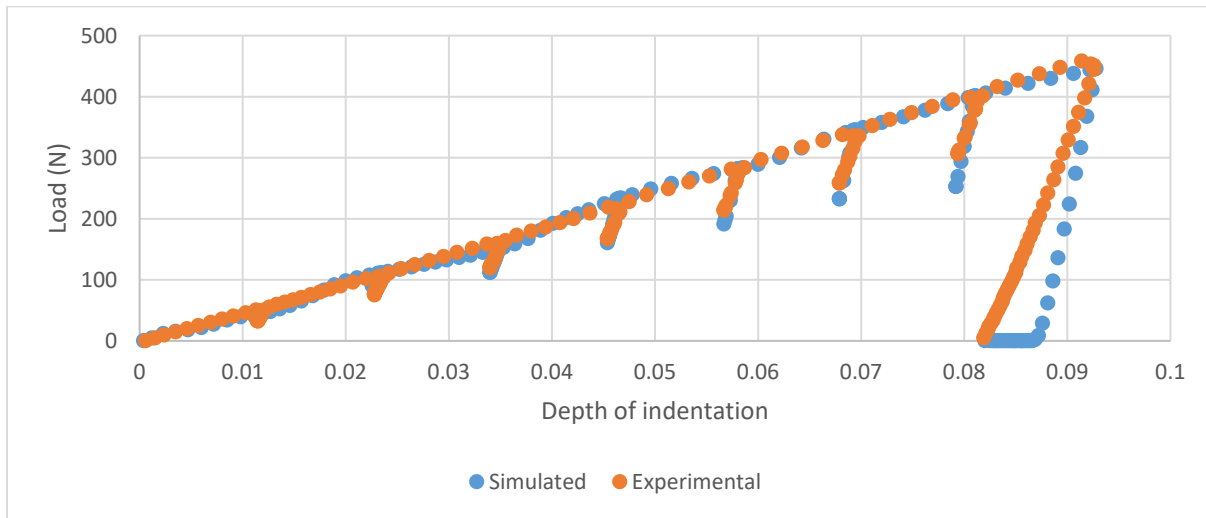


Figure 16. Overlay of experimental and simulation load vs. depth of indentation plots. A 20k node mesh with a peak indentation depth of 24% of indenter radius and a 20% unload at the end of each cycle was compared.

Conclusions

- The ABI analysis consistently under-predicted the yield strength values through indentation
- The Holloman’s power law was observed to be an invalid fit for true stress-true strain curve at low values of strain
- The Voce formulation was observed to be a good fit for estimating the entire flow curve.
- The ABI estimates for ultimate strength were close to the experimentally measured values
- The load vs. depth of indentation simulated using finite element methods, overpredicted the plastic deformation during the indentation

Acknowledgments

This work has been funded by Honeywell Federal Manufacturing & Technologies under Contract No. DE-NA0002839 with the U.S. Department of Energy. The United States Government retains and the publisher, by accepting the article for publication, acknowledges that the United States Government retains a nonexclusive, paid up, irrevocable, world-wide license to publish or

reproduce the published form of this manuscript, or allow others to do so, for the United States Government purposes. The supports from National Science Foundation Grants CMMI-1625736, and the Intelligent Systems Center (ISC) at Missouri S&T are greatly appreciated.

Furthermore, the authors would like to acknowledge Kyle Stagner, Ian Wille, and Brian Bullock for their aid in this research.

References

- [1] S.-W. Khoo, S. Karuppanan, C.-S. Tan, A Review of Surface Deformation and Strain Measurement Using Two-Dimensional Digital Image Correlation, *Metrol. Meas. Syst.* 23 (2016) 461–480.
- [2] M.B. Prime, Residual Stress Measurement by Successive Extension of a Slot: The Crack Compliance Method, *Appl. Mech. Rev.* 52 (1999) 75. doi:10.1115/1.3098926.
- [3] J. Laeng, J.G. Stewart, F.W. Liou, Laser metal forming processes for rapid prototyping - A review, *Int. J. Prod. Res.* 38 (2000) 3973–3996. doi:10.1080/00207540050176111.
- [4] C.A. Méndez, J. Cerdá, I.E. Grossmann, I. Harjunoski, M. Fahl, State-of-the-art review of optimization methods for short-term scheduling of batch processes, *Comput. Chem. Eng.* 30 (2006) 913–946. doi:10.1016/j.compchemeng.2006.02.008.
- [5] D.D. Gu, W. Meiners, K. Wissenbach, R. Poprawe, Laser additive manufacturing of metallic components: Materials, processes and mechanisms, *Int. Mater. Rev.* 57 (2012) 133–164. doi:10.1179/1743280411Y.0000000014.
- [6] A.E. Patterson, S.L. Messimer, P.A. Farrington, Overhanging Features and the SLM/DMLS Residual Stresses Problem: Review and Future Research Need, *Technologies.* 5 (2017) 15. doi:10.3390/technologies5020015.
- [7] B.C. Salzbrenner, J.M. Rodelas, J.D. Madison, B.H. Jared, L.P. Swiler, Y.-L.L. Shen, B.L. Boyce, High-throughput stochastic tensile performance of additively manufactured stainless steel, *J. Mater. Process. Technol.* 241 (2017) 1–12. doi:10.1016/j.jmatprotec.2016.10.023.
- [8] S. Karnati, I. Axelsen, F. F. Liou, J. W. Newkirk, Investigation Of Tensile Properties Of Bulk and SLM Fabricated 304L Stainless Steel Using Various Gage Length Specimens, in: *Proc. 27th Solid Free. Fabr. Symp.*, Austin, 2016: pp. 592–604.
- [9] S. Karnati, J.L. Hoerchler, F. Liou, J.W. Newkirk, Influence of Gage Length on Miniature Tensile Characterization of Powder Bed Fabricated 304L Stainless Steel, (n.d.). <https://sffsymposium.engr.utexas.edu/sites/default/files/2017/Manuscripts/InfluenceofGageLengthonMiniatureTensileChar.pdf> (accessed January 23, 2018).
- [10] M. Genest, M. Martinez, N. Mrad, G. Renaud, A. Fahr, Pulsed thermography for non-destructive evaluation and damage growth monitoring of bonded repairs, *Compos. Struct.* 88 (2009) 112–120. doi:10.1016/J.COMPSTRUCT.2008.02.010.
- [11] O.S. Salawu, Detection of structural damage through changes in frequency: a review, *Eng.*

- Struct. 19 (1997) 718–723. doi:10.1016/S0141-0296(96)00149-6.
- [12] J. García-Martín, J. Gómez-Gil, E. Vázquez-Sánchez, Non-Destructive Techniques Based on Eddy Current Testing, *Sensors*. 11 (2011) 2525–2565. doi:10.3390/s110302525.
- [13] B.W. Drinkwater, P.D. Wilcox, Ultrasonic arrays for non-destructive evaluation: A review, *NDT E Int.* 39 (2006) 525–541. doi:10.1016/J.NDTEINT.2006.03.006.
- [14] R.J. Schliekelmann, Non-destructive testing of adhesive bonded metal-to-metal joints 1, *Non-Destructive Test.* 5 (1972) 79–86. doi:10.1016/0029-1021(72)90099-0.
- [15] M. Ph Papaelias, C. Roberts, C.L. Davis, A review on non-destructive evaluation of rails: State-of-the-art and future development, *Proc. Inst. Mech. Eng. Part F J. Rail Rapid Transit.* 222 (2008) 367–384. doi:10.1243/09544097JRRT209.
- [16] F. Haggag, In-Situ Measurements of Mechanical Properties Using Novel Automated Ball Indentation System BT - In-Situ Measurements of Mechanical Properties Using Novel Automated Ball Indentation System, in: 1993.
- [17] F. Haggag, R. Nanstad, J. Hutton, D. Thomas, R. Swain, Use of Automated Ball Indentation Testing to Measure Flow Properties and Estimate Fracture Toughness in Metallic Materials BT - Use of Automated Ball Indentation Testing to Measure Flow Properties and Estimate Fracture Toughness in Metallic Materials, in: 1990.
- [18] K.L. Murty, M.D. Mathew, Nondestructive monitoring of structural materials using automated ball indentation (ABI) technique, *Nucl. Eng. Des.* 228 (2004) 81–96. doi:10.1016/J.NUCENGDES.2003.06.006.
- [19] T.S. Byun, J.H. Hong, F.M. Haggag, K. Farrell, E.H. Lee, Measurement of through-the-thickness variations of mechanical properties in SA508 Gr.3 pressure vessel steels using ball indentation test technique, *Int. J. Press. Vessel. Pip.* 74 (1997) 231–238. doi:10.1016/S0308-0161(97)00114-2.
- [20] M.. Mathew, K.. Murty, K.B.. Rao, S.. Mannan, Ball indentation studies on the effect of aging on mechanical behavior of alloy 625, *Mater. Sci. Eng. A.* 264 (1999) 159–166. doi:10.1016/S0921-5093(98)01098-3.
- [21] B.K. Choudhary, E.I. Samuel, K. Bhanu Sankara Rao, S.L. Mannan, Tensile stress–strain and work hardening behaviour of 316LN austenitic stainless steel, *Mater. Sci. Technol.* 17 (2001) 223–231. doi:10.1179/026708301101509890.
- [22] C.S. Kriewall, A.T. Sutton, S. Karnati, J.W. Newkirk, M.C. Leu, Effects of Area Fraction and Part Spacing on Degradation of 304L Stainless Steel Powder in Selective Laser Melting, in: n.d.
- [23] T. Amine, J. Newkirk, Elevated Temperature Microstructure Stability of Additive Manufactured 304L Stainless Steel, *Proc. 27th Solid Free. Fabr. Symp.* (2016, Austin, TX). (2016). http://scholarsmine.mst.edu/matsci_eng_facwork/2238 (accessed June 17, 2018).